JOURNAL OF Materials CHEMISTRY

Interesting transport and magnetic properties in a new family of molecular materials based on the organic donor BET-TTF and the perrhenate anion†

Salavat S. Khasanov,[a] Aarón Pérez-Benítez,[b,c] Bakhyt Zh. Narymbetov,[a] Leokadiya V. Zorina,[a] Rimma P. Shibaeva,[a] John Singleton,[d] Anne-Katrin Klehe,[d] Vladimir N. Laukhin,[b,e] José Vidal-Gancedo,[b] Jaume Veciana,[b] Enric Canadell[b] and Concepció Rovira*[b]

[a]*Institute of Solid State Physics, Russian Academy of Sciences, 142432 Chernogolovka, MD, Russia*
[b]*Institut de Ciència de Materials de Barcelona (CSIC), Campus Universitari de Bellaterra, E-08193, Cerdanyola, Spain. E-mail: cun@icmab.es; Fax: 935801853*
[c]*Universidad Autónoma de Puebla, 14 Sur y Av. San Claudio, San Manuel C. P. 725 70 Puebla, México*
[d]*Clarendon Laboratory, Parks Road, Oxford, UK OX1 3PU*
[e]*Institute of Problems of Chemical Physics, Russian Academy of Sciences, 142432 Chernogolovka, MD, Russia*

Received 10th July 2001, Accepted 21st November 2001
First published as an Advance Article on the web 30th January 2002

Three completely different salts, (BET-TTF)ReO_4 (**1**), (BET-TTF)$_3$(ReO_4)$_2$ (**2**), and (BET-TTF)$_9$(ReO_4)$_4$·2(THF) (**3**) are obtained by small variations in the electrocrystallization conditions of bis(ethylenethio)tetrathiafulvalene (BET-TTF) with the ReO_4^- ion. The crystal structures of the three salts show strong differences between them. In salt **1**, the completely ionic BET-TTF stacks, running along the *a* direction, are not regular but are forming weak dimers. Two different radical cation layers configure salt **2** and the analysis of the bond-length of BET-TTF molecules forming layers 1 and 2 shows that the β-like layer 1 has mixed valence character, while layer 2 can be regarded as an anion-cation-anion [ReO_4(BET-TTF)ReO_4]$^-$ sandwich layer with completely ionised BET-TTF. Only one β-like layer that consists of two different mixed valence stacks forms salt **3**. Conductivity measurements show that mixed valence salts **2** and **3** are metals with a metal-semiconductor transition around 125 K and 75 K respectively whereas the completely ionised salt **1** is, as expected, a semiconductor. The effect of high quasi-hydrostatic pressure and magnetic field on the transport properties of salt **3** has also been studied. The relationship between the crystal structure and the transport properties of all three salts has been analysed by means of tight binding band structure calculations. These calculations show that layer 1 is responsible for metallic conductivity of salt **2** whereas in layer 2 the electrons are localised. EPR data of this salt indicate that there is an appreciable interaction between delocalised electrons in layer 1 and localised magnetic moments in layer 2.

Introduction

Since the discovery of superconductivity in organic radical cation salts[1] a large number of organic metals and superconductors have been prepared. Of these compounds a great majority have the donor molecule bis(ethylenedithio)tetrathiafulvalene (BEDT-TTF) as the organic component.[2] This donor provided the first sulfur based superconductor (BEDT-TTF)$_2$$ReO_4$ (T_c = 2 K at 4.5 kbar)[3] as well as the superconductor κ-(BEDT-TTF)$_2$Cu[N(CN)$_2$]Cl with the present record critical temperature (T_c = 12.8 K at 0.3 kbar).[4] The external sulfur atoms of the BEDT-TTF molecule as well as the ethylene groups play a key role in the establishment of the appropriate crystal packing, since it has been stated that S···S and C–H···S interactions are very useful as secondary interactions in order to achieve supramolecular assemblies of TTF derivatives.[2,5] In addition, it is well known that the S···S interstack overlap promotes a higher electronic dimensionality in a great number of conductors and superconductors.[2]

Bis(ethylenethio)tetrathiafulvalene (BET-TTF) is a similar TTF building block that maintains the characteristics of BEDT-TTF. BET-TTF can be regarded as derived from BEDT-TTF by elimination of one of the sulfur atoms of the external six-membered rings.

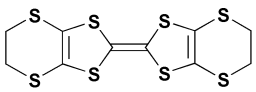

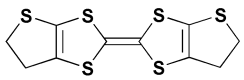

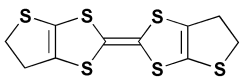

Thus, in BET-TTF the ethylene groups as well as one sulfur atom remain in the same position as in BEDT-TTF. Nevertheless, the five-membered rings in BET-TTF are much more rigid than the six-membered rings of BEDT-TTF and the conformational isomerism due to ethylene groups is not

†Electronic supplementary information (ESI) available: overlap modes of the radical cations of **1**–**3**. See http://www.rsc.org/suppdata/jm/b1/b106070h/

 DOI: 10.1039/b106070h

possible in BET-TTF salts. By contrast, BET-TTF exists in *E* and *Z* conformations. In accordance with the structural and electronic characteristics of BET-TTF, this donor forms crystalline radical-ion salts with tetrahedral, octahedral, linear or monoatomic anions showing different crystallographic motifs (α, β, κ or θ type packing) very similar to those of the BEDT-TTF salts.[6,7,8,9] In all mixed valence BET-TTF salts the donor forms layers sustained by S···S and C–H···S contacts that are separated by layers of anions and that have good metallic properties. A broad metal-insulator (M–I) transition is observed in most of these salts which has been attributed to electron localisation due to the disorder of the BET-TTF donors in the crystals. This assumption is consistent with the observation of a stable metallic character in $(BET\text{-}TTF)_2X\cdot 3H_2O$ (X = Br, Cl) in which only completely ordered (*E*)-BET-TTF donors are found in the cationic layer. In addition, the indication of a superconducting transition has been observed in two crystals of the bromide salt.[9]

It is therefore of interest to prepare salts of the BET-TTF donor with the perrhenate ion, ReO_4^-. This anion formed a rich family of five ion radical salts with the BEDT-TTF donor with different packing motifs (α, β and γ) and transport properties ranging from semiconductors to superconductors.[3,10,11,12] In addition, the ReO_4^- ion also gives rise to a superconducting salt with the related donor BEDO-TTF.[13] In this paper we present the synthesis, structural, electronic and physical characterization of three new radical cation salts obtained by the combination of the BET-TTF donor with the ReO_4^- ion.

Results and discussion

Synthesis

By electrocrystallization of the BET-TTF donor at Pt wire electrodes, using tetraalkylammonium perrhenate as electrolyte, three different salts were obtained depending on the solution polarity (Table 1). When a solution of Bu_4NReO_4 in dry THF was used, brown plates of the $(BET\text{-}TTF)_3(ReO_4)_2$ salt (**2**) were obtained. With the more polar solution THF–EtOH (11 : 1 v/v), black prisms of the completely ionic salt $(BET\text{-}TTF)ReO_4$ (**1**) grew on the anode. The use of THF–H_2O (11 : 1 v/v) solutions led to black rulers of the mixed valence salt $(BET\text{-}TTF)_9(ReO_4)_4\cdot 2THF$ (**3**).[14] In some experiments, salts **1** and **2** were obtained in the same cell, reflecting the fact that a very small variation in solvent polarity drives the formation of one or the other salt.

Whereas the 9 : 4 donor : anion ratio found in salt **3** is novel for the family of BET-TTF salts, stoichiometries of 1 : 1 and 3 : 2 had been obtained previously. There are some similarities between the latter and salts obtained with the ReO_4^- anion and the BEDT-TTF donor, for which several 3 : 2 phases as well as a mixed valence salt containing THF, $(BEDT\text{-}TTF)_2ReO_4\cdot 0.5THF$, are known.[10–12] Whereas for $(BEDT\text{-}TTF)_3(ReO_4)_2$, three different crystallographic phases (α, β and γ), and for the salts with a 2 : 1 stoichiometry, two phases have been obtained,[3,10–12] only one crystallographic phase of each of the $(BET\text{-}TTF)(ReO_4)$ (**1**), $(BET\text{-}TTF)_3(ReO_4)_2$ (**2**), and $(BET\text{-}TTF)_9(ReO_4)_4\cdot 2THF$ (**3**) salts has been discovered so far.

Table 2 Crystal data and structure determination details for salts **1–3**

Compound	$(BET\text{-}(ReO_4)$ (**1**)	$(BET)_3\text{-}(ReO4)_2$ (**2**)	$(BET)_9(ReO_4)_4\cdot$ 2THF (**3**)
Formula	$C_{10}H_8O_4\text{-}ReS_6$	$C_{30}H_{24}O_8\text{-}Re_2S_{18}$	$C_{98}H_{88}O_{18}\text{-}Re_4S_{54}$
M	570.7	1462	4029.7
Crystal system	Triclinic	Triclinic	Triclinic
a/Å	7.760(8)	6.370(2)	10.993(3)
b/Å	8.890(5)	7.788(4)	19.292(4)
c/Å	12.325(4)	22.865(5)	17.713(4)
α/°	73.95(4)	84.60(3)	120.96(2)
β/°	113.47(5)	89.50(2)	89.76(3)
γ/°	87.31(6)	70.25(3)	91.88(3)
V/Å^3	737.5(9)	1062.5(7)	3219(1)
T/K	293(2)	293(2)	293(2)
Space group	$P\bar{1}$	$P\bar{1}$	$P\bar{1}$
Z	2	1	1
μ/cm^{-1}	90.96	66.25	46.90
No. of reflns measured	3600	2337	3528
No. of independent reflns	2658	2149	3230
$R_{int.}$	0.020	0.044	0.043
No. of obsd reflns	2509	1868	3173
R	0.065	0.072	0.061
R_w	0.193	0.146	0.121

Crystal structure

Although most of the crystals collected on the anode of the different electrocrystallisation cells were of poor quality, some crystals of the three salts could be used for X-ray structure determinations (Table 2). The crystal structure of salt **1** (see Fig. 1) is characterised by the presence of BET-TTF stacks running along the *a*-direction. The stacks are not regular but are divided into dimers with interplanar spacings of 3.40 Å and 3.64 Å for $I\text{-}I_{ia}$ and $I\text{-}I_i$, respectively, which correspond to the intra- and interdimer distances. There are many short intradimer S···S (⩽3.70 Å), S···C (⩽3.65 Å) and C···C (⩽3.60 Å) distances, but no interdimer contacts within the stacks. Only six interstack contacts were discovered. There is a pronounced cation–anion interaction evidenced by the presence of many short S···O and C···O contacts between the BET-TTF and ReO_4. The BET-TTF molecules in $(BET\text{-}TTF)ReO_4$ are approximately planar showing only a small distortion toward a chair

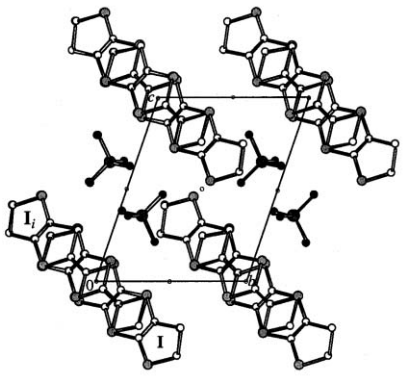

Fig. 1 Projection of the structure of $(BET\text{-}TTF)\cdot ReO_4$ (**1**) along the *a*-direction.

Table 1 Conditions for the electrocrystallization of salts **1–3**

Salt	Solvent[a]	*I*/μA	Time/days	Aspect
$(BET\text{-}TTF)ReO_4$ (**1**)	THF : EtOH (11 : 1)	0.5	12	Black prisms
$(BET\text{-}TTF)_3(ReO_4)_2$ (**2**)	THF	1–1.2	4	Brown plates
$(BET\text{-}TTF)_9(ReO_4)_4\cdot 2THF$ (**3**)	THF : H_2O (11 : 1)	0.5	12	Brown rulers

[a]THF = tetrahydrofuran; EtOH = ethanol.

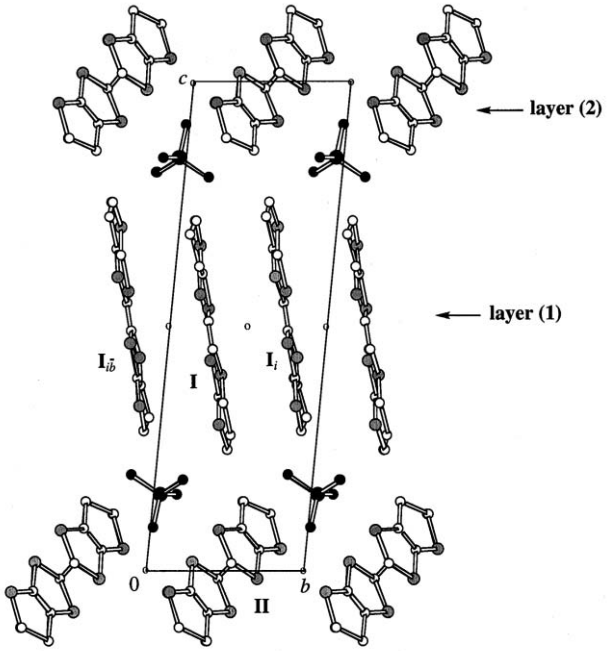

Fig. 2 Projection of the structure of $(BET\text{-}TTF)_3(ReO_4)_2$ (**2**) along the *a*-direction.

conformation. The angles between the external rings and the mean plane of the TTF core double bonds are 1.5° and 4.8°. Almost the same deviation from planarity has been found in the neutral donor[15] as well as in the (BET-TTF) $AuBr_2$ salt.[16] It should be noted that the completely ionic salt **1** is not isostructural with any other 1 : 1 BET-TTF salt such as (BET-TTF)$AuBr_2$[16] or (BET-TTF)SCN.[8]

Fig. 2 shows a projection of the crystal structure of salt **2** along the *a*-direction. The structure is characterized by the presence of two different radical cation layers parallel to the *ab* plane. Layers 1 (see Fig. 2), which are built exclusively from BET-TTF donors, alternate along the *c*-direction with sandwich layers of $[ReO_4(BET\text{-}TTF)ReO_4]^-$ (from now on referred to as layers 2). In the structure there are thus two crystallographically nonequivalent BET-TTF molecules, I and II, associated with layers 1 and 2 respectively. Whereas one of them (I) lies in a general position, the other (II) is located at a symmetry center. The BET-TTF molecules I and II differ somewhat in their conformation. For molecule I the angles between the external rings and the planar TTF core are 0.3° and 3.6°. One of the external five-membered rings has a chair conformation and the other is planar. The TTF core of molecule II is not completely planar since the two moieties are not coplanar, the interplanar spacing being 0.12 Å. The external five-membered rings are almost planar, one CH_2 group (envelope form) exhibiting a very small deviation (0.23 Å).

The bond length distribution differs in the radical cations I and II. Although the poor accuracy in the determination of the interatomic distances (±0.02–0.03 Å) does not allow a detailed analysis, some important conclusions can be drawn. For instance, the length of the central C=C bond in radical cation I, 1.34(3) Å, is close to the length of the same bond in other BET-TTF salts having $(BET\text{-}TTF)^{0.5+}$ as a component.[7,17] This bond is larger in radical cation II (1.46(3) Å) whose bond length is similar to that observed in the central C=C bonds in $(BET\text{-}TTF)^{1+}$ salts. In agreement with their charges, the $S\text{–}C_{sp^2}$ bonds in molecule I are longer than in molecule II. Therefore, it can be concluded that layer 2 contains completely ionized BET-TTF molecules whereas on average two molecules of BET-TTF in layer 1 jointly donate one electron to the anion layer, thus having a mixed valence character.

The projection of the radical cation layer 1 along the

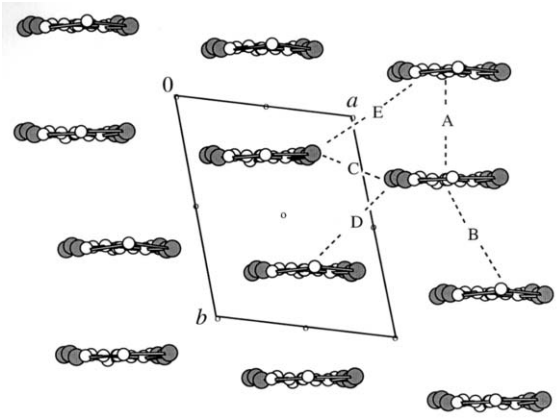

Fig. 3 Projection of the radical cation layer 1 of $(BET\text{-}TTF)_3(ReO_4)_2$ (**2**) along the *c*-direction.

c-direction is shown in Fig. 3: a β-type layer of BET-TTF stacks parallel to the *b*-direction can be seen. The interplanar separations are 3.80 and 3.63 Å for I-I_i and I-I_{ib}, respectively. There are no S···S or S···C contacts shorter than the sum of the van der Waals radii within the stacks, but there are a large number of short side-by-side contacts in the *a*-direction. Fig. 4 shows the projection of the mixed cation–anion $[ReO_4(BET\text{-}TTF)ReO_4]^-$ sandwich layer along the *c*-direction. In this layer the $(BET\text{-}TTF)^{1+}$ radical cations are practically not interacting with each other. However, there is a pronounced interaction between $(BET\text{-}TTF)^{1+}$ and ReO_4^- since every cation II has twelve short S···O and C···O contacts with the anion.

The crystal packing of the radical cation salt $(BET\text{-}TTF)_3(ReO_4)_2$ (**2**) is completely different from that of the 3 : 2 salt of BET-TTF with the PF_6^- and AsF_6^- anions (α type packing).[7,17] In fact, the physical properties of $(BET\text{-}TTF)_3(ReO_4)_2$ should be compared with those of the family of salts $(BET\text{-}TTF)_2X$ (X = PF_6, AsF_6, SbF_6 and SCN) because their conducting layers have the same composition $[(BET\text{-}TTF)^{0.5+}]_2$ and packing (β type).[7] It should be noted that the crystal packing found in $(BET\text{-}TTF)_3(ReO_4)_2$ is very similar to that in the $(BEDT\text{-}TTF)_3(ZnCl_4)_2$ salt.[18] However, in this salt there are layers of the completely ionic $(BEDT\text{-}TTF)^{1+}$ species alternating with the mixed layers $[ZnCl_4(BEDT\text{-}TTF)^{2+}ZnCl_4]^{2-}$ and this is why the latter salt is not conducting.

The X-ray analysis of salt **3** shows that it has the composition $(BET\text{-}TTF)_9(ReO_4)_4{\cdot}2THF$.[14] The projection of the crystal structure of **3** along the *a*-direction is shown in Fig. 5. The

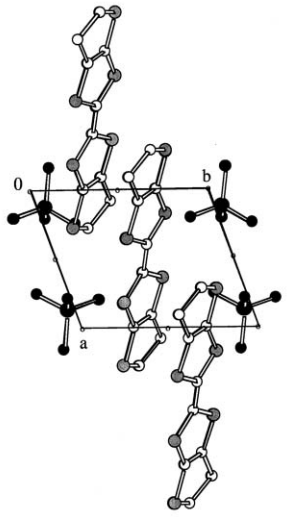

Fig. 4 Projection of the $[ReO_4(BET\text{-}TTF)ReO_4]^{1-}$ sandwich layer 2 of $(BET\text{-}TTF)_3(ReO_4)_2$ (**2**) along the *c*-direction.

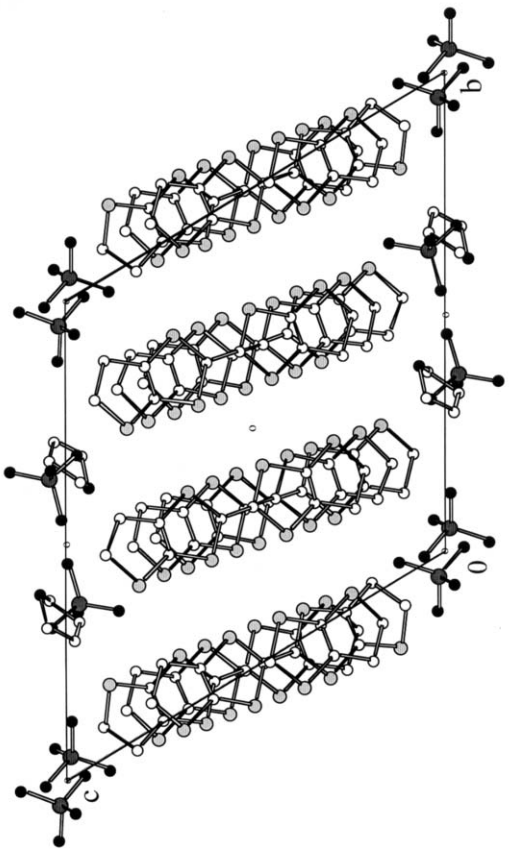

Fig. 5 Projection of the structure of $(BET\text{-}TTF)_9(ReO_4)_4{\cdot}2THF$ (**3**) along the *a*-direction.

structure is characterized by the presence of radical cation layers parallel to the *ab* plane, alternating along the *c* plane with layers of the ReO_4^- anions and tetrahydrofuran molecules. A projection of the radical cation layer along the *c*-direction is shown in Fig. 6. It is constructed of two non-equivalent stacks parallel to the *a*-axis. Radical cations I and II form one of the stacks, the other stack consisting of radical cations III, IV and V. The mean planes of the radical cations are not completely parallel to each other; the dihedral angles formed by the planes of different radical cations are 1.8, 0.8, 1.4 and 1.7° for I-II, III-V, V-IV and III-IV, respectively. All pairs of donors show the same ring-over-bond overlap mode. The stacks are bound together by a network of short S···S contacts between neighboring BET-TTF molecules.

The X-ray study has shown that there is positional disorder in the sulfur atoms of the external rings of BET-TTF molecules

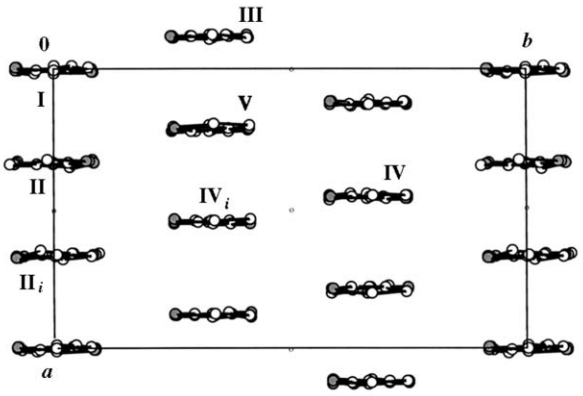

Fig. 6 Projection of the radical cation layer of $(BET\text{-}TTF)_9(ReO_4)_4{\cdot}2THF$ (**3**) along the *c*-direction.

of the three salts. This was evident from the occupation factors of the corresponding sulfur and carbon atoms. This fact is quite common in the crystal structures of BET-TTF molecular solids, and has been observed both in the neutral donor[15] and in salts with different stoichiometries.[6–8,17] It may arise from the coexistence of *cis* and *trans* isomers of the BET-TTF cations in the crystal due to an isomerization of the initially *trans* BET-TTF during the oxidation process. A second contribution to the disorder may be due to the two possible ways of packing of the BET-TTF molecules in the structure. Up to now, completely ordered layers with the *trans*-configuration (*i.e.*, the *E*-isomer) for this donor have only been observed in the $(BET\text{-}TTF)[AuBr_2]$,[17] $(BET\text{-}TTF)[Au(mnt)_2]$[19] and $(BET\text{-}TTF)_2X{\cdot}3H_2O$ (X = Br, Cl) salts.[9] The BET-TTF molecules in these crystals are located at inversion centers and the peripheral sulfur atoms have the occupation factor 1. In the present case, it is only possible to conclude that the BET-TTF molecules of type II in $(BET\text{-}TTF)_3(ReO_4)_2$ salt and the BET-TTF molecules of type I in $(BET\text{-}TTF)_9(ReO_4)_4{\cdot}2THF$ salt have a *trans*-configuration (*E*-isomer).

Electronic structure

In order to gain some insight into the correlation between the crystal structure and the transport properties (see following section) of the three BET-TTF salts reported here, we carried out tight binding band structure calculations on their donor lattices. The donor layers of the 1 : 1 salt **1** are built from chains of dimers along the *a*-direction which stack along the (*b*–*c*)-direction. Taking into account S···S and S···C contacts shorter than 4.0 and 3.7 Å, respectively, there are two different donor···donor interactions within the stacks (intra- and interdimer) and two interactions between the stacks. In order to quantify the strength of the HOMO···HOMO interactions associated with them we calculated the so-called $\beta_{HOMO\text{–}HOMO}$ interaction energies.[20] Those associated with the chain [0.513 eV (intradimer) and 0.233 eV (interdimer)] are considerably larger than those of the two interstack interactions [0.053 and 0.003 eV]. This suggests a strong one-dimensional character for salt **1**, in agreement with the EPR measurements (see next sections). Although these measurements clearly show that salt **1** behaves as a normal 1 : 1 salt, *i.e.*, it is a localized semiconductor, the large difference between the two interactions along the chain suggests the possibility of a transition to a semiconducting and nonmagnetic state. However, the transport property measurements clearly show that this transition does not occur. Most likely, the interactions with the ReO_4^- anions make the donor lattice too stiff to allow for an increase in the structural dimerization which would stabilize the nonmagnetic state.

As mentioned in the previous section, the crystal structure of salt **2** can be considered to be built from two types of layers. As far as the HOMO bands are concerned, the ReO_4^- anions do not play any significant role so that only the donor sublattice of layer 2 will be considered in our discussion. Both layers are built from just one independent BET-TTF donor. The calculated HOMO energy for the donor in layers 1 and 2 is −8.575 and −8.266 eV, respectively. Even taking into account the modest accuracy in the crystal structure determination, such a large difference, together with the large difference in the central C=C bond lengths, strongly suggests that donors in layers 1 and 2 are really $(BET\text{-}TTF)^{0.5+}$ and $(BET\text{-}TTF)^{1+}$, respectively. Layer 2 can be considered to consist of independent uniform chains because there are no short S···S or S···C intermolecular contacts between these chains. The calculated $\beta_{HOMO\text{–}HOMO}$ interaction energy for the only intermolecular contact of the uniform chain is 0.092 eV, a relatively low value, clearly smaller than those of the chains in salt **1**, for instance. Altogether, these observations suggest that layer 2 should be considered as a series of independent chains of

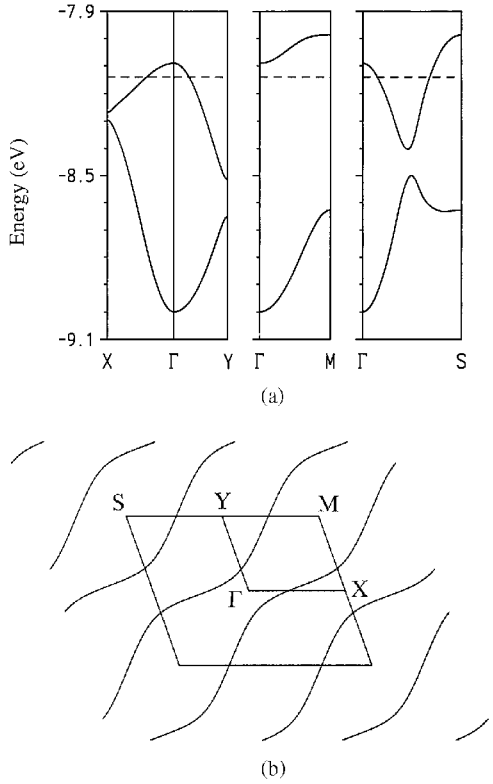

Fig. 7 Band structure (a) and Fermi surface (b) calculated for layer 1 of the $(BET\text{-}TTF)_3(ReO_4)_2$ salt, assuming an ordered distribution of donors. The dashed line in (a) refers to the Fermi level and $\Gamma = (0, 0)$, $X = (a^*/2, 0)$, $Y = (0, b^*/2)$, $M = (a^*/2, b^*/2)$ and $S = (-a^*/2, b^*/2)$.

weakly interacting $(BET\text{-}TTF)^{1+}$ units and thus, it should have an activated and not very large contribution to the conductivity of salt **2**.

To calculate the electronic structure of layer 1 of salt **2** the positional disorder in the sulfur atoms of the external rings was ignored; *i.e.*, an ordered lattice was used in which every position was assumed to contain the donor in the major conformation and orientation as determined in the X-ray analysis. The possible influence of disorder on the electronic structure was considered by repeating the calculations for a lattice in which the five-membered rings were replaced by two hydrogen atoms, *i.e.*, for a lattice of TTF donors with exactly the same geometry as in the crystal structure of **2**. The calculated band structure for the ordered lattice of BET-TTF donors is shown in Fig. 7a. It contains two quite dispersive HOMO bands, the upper one being half-filled. When the outer five-membered rings of the donors are disregarded, the total bandwidth is only 15% smaller than that of Fig. 7a. Since this calculation should give a lower limit for the band dispersion, it can be concluded that disorder only very slightly affects such dispersion. Thus, the band dispersion of the partially filled band of layer 1 is quite large and salt **2** should be metallic. This prediction is in agreement with the resistivity measurements reported in the next section.

The calculated Fermi surface is reported in Fig. 7b. The shape of this surface is practically unchanged when the outer five-membered rings are disregarded in the calculations. Thus, the Fermi surface of Fig. 7b is the appropriate one in order to discuss the transport properties of salt **2**. This surface is a quite warped pseudo one-dimensional one and exhibits an almost perfect $a^*/2$ nesting vector. The existence of warped but nevertheless open lines perpendicular to the $(-a + b)$-direction may seem at first sight surprising because apparently there are no chains along this direction in layer 1 (see Fig. 3). However, this fact can be easily understood when the strength of the different donor···donor interactions is taken into account. There are five different intermolecular interactions in layer 1 (see Fig. 3). The absolute values of the $\beta_{HOMO\text{–}HOMO}$ interaction energies are 0.358 (**A**), 0.069 (**B**), 0.148 (**C**), 0.269 (**D**) and 0.087 (**E**) eV. The fact that interaction **A** is the largest one and that there is a large difference between interactions **A** and **B** suggests that, as far as the HOMO···HOMO interactions are concerned, the stacks along the *b*-direction can be described as stacks of dimers. In addition, interaction **D** is the second largest one and interactions **C** and **E**, which also couple the stacks of dimers, are quite sizeable but smaller than **D**. Since the dimers are coupled along the $(-a + b)$ direction by interaction **D**, as far as the HOMO···HOMO interactions are concerned, layer 1 of salt **2** can be described as a series of moderately interacting chains of dimers along the $(-a + b)$-direction. The shape of the Fermi surface naturally reflects this situation.

As mentioned already, the Fermi surface of layer 1 exhibits an almost perfect nesting vector so that it could be expected that structural modulation could destroy the metallic character of salt **2**. However, we do not believe that this is the origin of the metal-insulator transition of this salt because the resistivity upturn in the resistivity *vs.* temperature measurements (see Fig. 10) is quite broad. A progressive localization of the carriers seems to be a more likely explanation for the resistivity upturn in salt **2**. In conclusion, it seems that the disorder exhibited by the donor lattice of **2**, even if it does not destroy the metallic character around room temperature, really does so at lower temperatures. In so doing it masks the inherent instability of the lattice towards dimerization, which would also destroy the metallic properties of this salt.

The repeat unit of the donor lattice of salt **3** contains nine donors and consequently, the band structure of this salt contains nine HOMO bands (see Fig. 8a; exactly as for salt **2**, an ordered lattice of BET-TTF donors was assumed in our calculations). There are fifteen different donor···donor

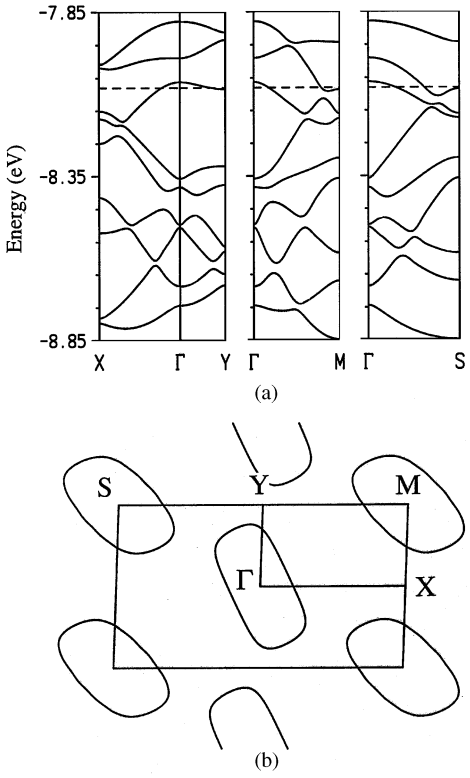

Fig. 8 Band structure (a) and Fermi surface (b) calculated for the donor lattice of $(BET\text{-}TTF)_9(ReO_4)_4{\cdot}2THF$, assuming an ordered distribution of donors. The dashed line in (a) refers to the Fermi level and $\Gamma = (0, 0)$, $X = (a^*/2, 0)$, $Y = (0, b^*/2)$, $M = (a^*/2, b^*/2)$ and $S = (-a^*/2, b^*/2)$.

interactions in the lattice so that it is not very informative to consider the actual values of the $\beta_{HOMO-HOMO}$ interaction energies for all these interactions. Similar to the case of salt **2**, the total width of the HOMO bands in salt **3** is approximately 1 eV, indicating quite a large interaction. Given the stoichiometry of the salt, there must be four holes in the nine HOMO bands of the donor lattice. Thus, in principle, salt **3** could be a semiconductor or a metal depending on the existence or absence of an energy gap between the second and the third upper HOMO bands. As shown in Fig. 8a, these bands overlap, in agreement with the conductivity measurements reported in the next section showing that salt **3** is a metal at room temperature.

As shown in Fig. 8b, the Fermi surface of this salt contains closed sections with a cross sectional area of 14.8% of the Brillouin zone around Γ (hole pockets) and M (electron pockets). The shape of the Fermi surface is not changed when the outer five-membered rings are disregarded in the calculations. As was found for salt **2**, the disorder of the donor lattice seems to play a very minor role in the electronic structure of this salt. It is interesting to note that the shape of the two closed sections is such that they can not be superposed. Consequently, it is not expected that a structural modulation could destroy the metallic state of this salt. The resistivity *vs.* temperature measurements (see Fig. 10) exhibit however an upturn in the resistivity at around 75 K. Two possible mechanisms by which the metallic conductivity of this salt can be completely or partially destroyed are the following. First, because of band dispersion in the region where the band overlap is not so large, relatively small structural changes may totally or partially destroy the band overlap and thus affect the conductivity. It is quite likely that the interesting conductivity behavior of this salt under pressure (see next section), at least partially, results from the progressive destruction of the band overlap as a result of slight pressure induced structural changes. Second, as it was the case for salt **2**, the disorder exhibited by the donor lattice may lead to electron localization. According to the EPR measurements, this is the more likely origin for the low temperature activated behavior at normal pressure. It is clear that there exists a very subtle balance between different electronic states (metallic with different degrees of band overlap, band gap on localised semiconducting states) which can be altered by the effect of temperature and/or pressure, as suggested by the transport measurements reported in the next section.

Transport properties

Fig. 9 shows the temperature dependence of the resistance normalised by the room temperature value for the simple 1 : 1 salt (BET-TTF)(ReO_4) (**1**). As expected, this compound is a semiconductor (room temperature conductivity $\sigma \approx 0.05\ \Omega^{-1}\ cm^{-1}$ and activation energy $E_a \approx 0.127$ eV).

The temperature dependence of the normalised resistance for the two salts with mixed valence character (**2** and **3**) is presented in Fig. 10. The room temperature conductivity is about 20–30 $\Omega^{-1}\ cm^{-1}$ for salt **2** while it is about one order of magnitude larger for salt **3** (in the range 100–400 $\Omega^{-1}\ cm^{-1}$). Both of them show a metallic-like behaviour down to 125 K and 75 K, respectively. Below these temperatures a phase transition to a non-metallic state takes place. However, we should note that these low temperature phases do not seem to be dielectric as they are for other salts in which the resistivity dramatically increases by many orders of magnitude when the temperature decreases a few degrees (*e.g.* for the α-(BEDT-TTF)$_2I_3$ salt).[21] For the materials studied, the low temperature resistance increases by only one order of magnitude when the temperature decreases by a factor of about 100. For this reason, the low temperature state of these salts could be considered as a semimetallic state. Moreover, it is worth noting that in the case of salt **3** the resistance below 75 K increases gradually, while for

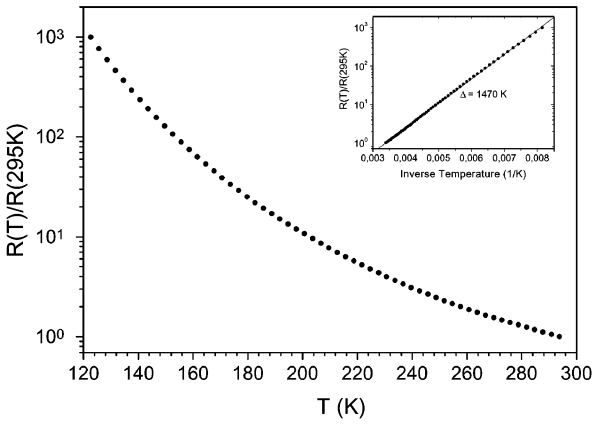

Fig. 9 Temperature dependence of the normalised resistance of the (BET-TTF)(ReO_4) salt (**1**). The inset shows the same resistance in a logarithmic scale *vs.* inverse temperature.

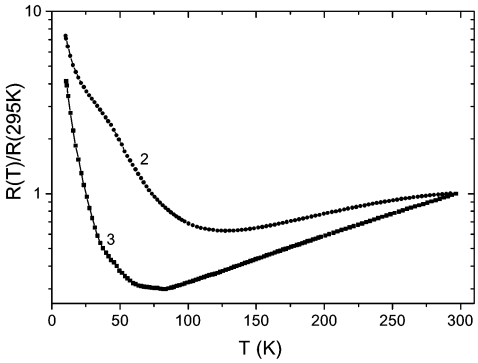

Fig. 10 Temperature dependence of the normalised resistance of the mixed valence salts (BET-TTF)$_3$(ReO_4)$_2$ (**2**) and (BET-TTF)$_9$-(ReO_4)$_4$·2THF (**3**).

the salt **2** the increase in the resistance below 125 K occurs in two steps, which could originate from two low temperature phase transitions. This is also reflected in a non-monotonous increase in the spin susceptibility at low temperatures (see Fig. 15b below). At the present time the origin of that behaviour is not clear (although the fact that two different subsystems can contribute to the conductivity of this salt probably lies at the origin of this puzzling behavior). The low temperature behaviour of salt **2** is under further investigation.

Let us consider now some preliminary experimental results related to the effects of high quasi-hydrostatic pressure and magnetic field on the transport properties of salt **3**. Fig. 11 shows the pressure dependence of the resistance at room temperature for one of the crystals of the (BET-TTF)$_9$-(ReO_4)$_4$·2THF salt.[22] Initially, the resistance of the sample

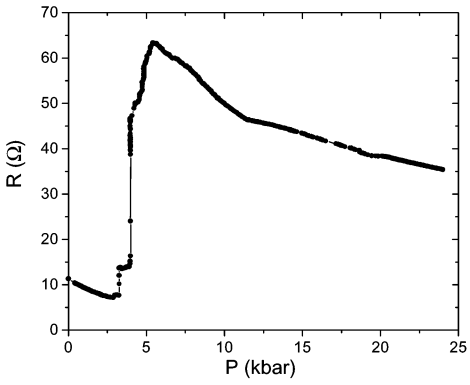

Fig. 11 Pressure dependence of the room temperature resistance for one of the crystals of the (BET-TTF)$_9$(ReO_4)$_4$·2THF salt.

decreases when pressure is applied. However, at $P \approx 4$–5 kbar the resistance abruptly increases by a factor of up to seven, indicating a first order phase transition to a high pressure phase. Usually, a higher pressure phase should have shorter inter- and intrastack contacts and consequently, lower in-plane resistivity. Thus, this behavior is far from usual. It could be suggested that at the phase transition some sliding of the BET-TTF molecules in the stacks plays an important role and dominates over the decrease of the interstack distances. In that case, the effective overlap can decrease and thus lead to higher resistivity of the high-pressure phase observed in Fig. 11. Due to the large number of transfer integrals in the layer it is however very difficult to provide an adequate explanation along this line. Analysis of a crystal structure under pressure is required before a real understanding of the mechanism of this phase transition can be attained.

Fig. 12 shows the temperature dependence of the resistance normalised by the room temperature value (R_N) at a given pressure for the high-pressure phase of salt **3**. Under moderate pressures ($P \leqslant 11$ kbar), a well pronounced jump in the resistance during the cooling process is observed (for details see inset **a** in Fig. 12). This jump can be considered as an indication for a new first order phase transition occurring just below room temperature and resulting in a stabilization of a lower resistance and metallic-like phase, the temperature of this transition rising with increasing pressure. A low-temperature phase transition still exists for this phase, the transition temperature shifting to lower temperatures when the pressure increases. This higher resistance state at the lowest temperature seems to be suppressed by a higher pressure (see Fig. 12, main panel). However, the increase of pressure above ≈ 12 kbar probably stabilizes another higher pressure phase, for which practically no pressure effect on the $R_N(T)$ dependence was observed over the temperature range studied (*i.e.*, $2 < T < 300$ K, see inset **b** in Fig. 12). The stabilization of this phase by the higher pressure is probably also reflected in a change of the slope around $P \approx 12$ kbar in the $R(P)$ dependence (see Fig. 11).

In order to get more information about the transport properties of the low-temperature state of this high-pressure phase we have carried out magnetoresistance measurements of the crystals in a magnetic field of up to 16 T directed perpendicular to the conducting planes and under quasi-hydrostatic pressure in the range $15 \leqslant P \leqslant 22$ kbar. Fig. 13 shows the field dependence of the magnetoresistance (MR) at 1.9 K normalised by the zero field value at a given pressure for

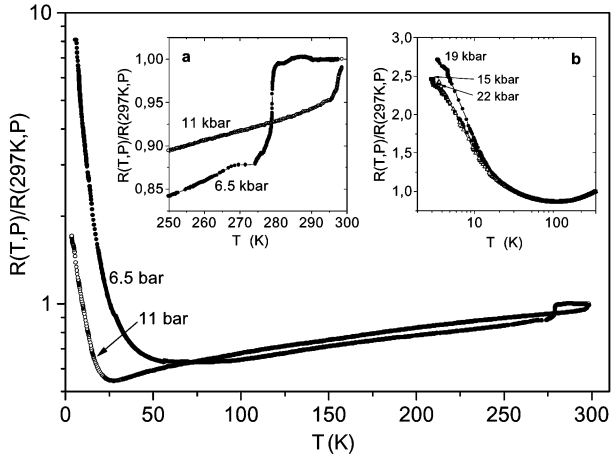

Fig. 12 Temperature dependence of the resistance normalised by the room temperature value at the given pressure ($5 < P < 12$ kbar) for the high pressure phases of the (BET-TTF)$_9$(ReO$_4$)$_4$·2THF salt; inset **a**: details of the high temperature region; inset **b**: the same dependence for $P > 12$ kbar (see text). All indicated pressures are fixed at room temperature.

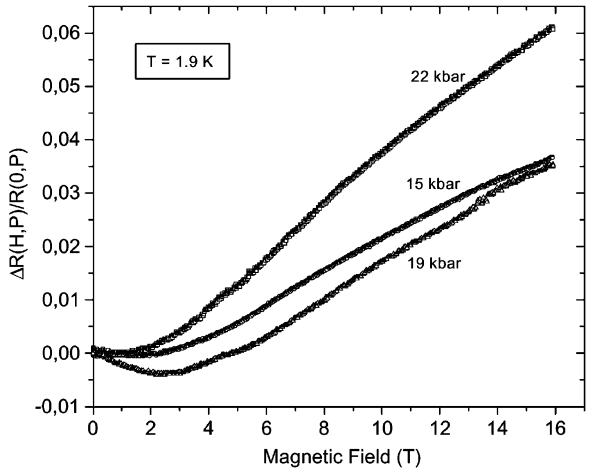

Fig. 13 Magnetic field dependence of the magnetoresistance at $T = 1.9$ K of the salt (BET-TTF)$_9$(ReO$_4$)$_4$·2THF for three different pressures normalised by the zero field value at a given pressure.

three different pressures. In contrast with the expected monotonous pressure dependence of the MR, as for instance for (BEDO-TTF)$_2$ReO$_4$·H$_2$O,[23] we found unconventional non-monotonous behaviour of the MR *vs.* pressure in the same pressure range where no pressure dependence of the $R_N(T)$ was detected (see inset **b** in Fig. 12). The MR is small at 15 kbar (only about 3% at 16 T) and after initially slightly decreasing with increasing pressure the MR increases up to $\approx 6\%$ at 22 kbar. The origin of this is not clear at present and additional measurements are needed.

According to the band structure calculations (see above), the Fermi surface (FS) of salt **3** at ambient pressure consists of two types of closed pockets. However, no Shubnikov–de Haas (SdH) oscillations were observed in magnetic fields of up to 16 T at temperatures as low as 1.9 K. Much higher field or/and lower temperatures are probably required for the observation of SdH oscillations in this material.

In contrast to semi-classical expectations[24] the normalized MR in (BET-TTF)$_9$(ReO$_4$)$_4$·2THF decreases with decreasing temperature, as can be observed in Fig. 14. This unconventional behaviour could be associated with some additional (negative) contribution to the semiclassical galvanomagnetic mechanism of the normal (positive) MR, for example some delocalisation of electrons/holes by the magnetic field which can be increased by lowering the temperature. Moreover, this contribution resulting from a field induced delocalising effect

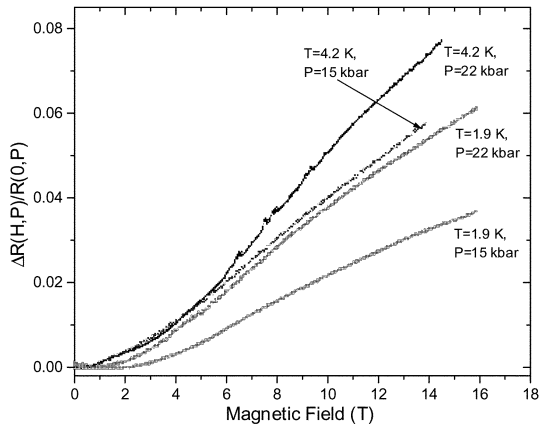

Fig. 14 Field dependence of the magnetoresistance for the (BET-TTF)$_9$(ReO$_4$)$_4$·2THF salt under pressures $P = 15$ kbar and 22 kbar at two temperatures $T = 4.2$ and 1.9 K. The magnetoresistance was normalised by the zero field value at a given pressure. All indicated pressures given are fixed at room temperature.

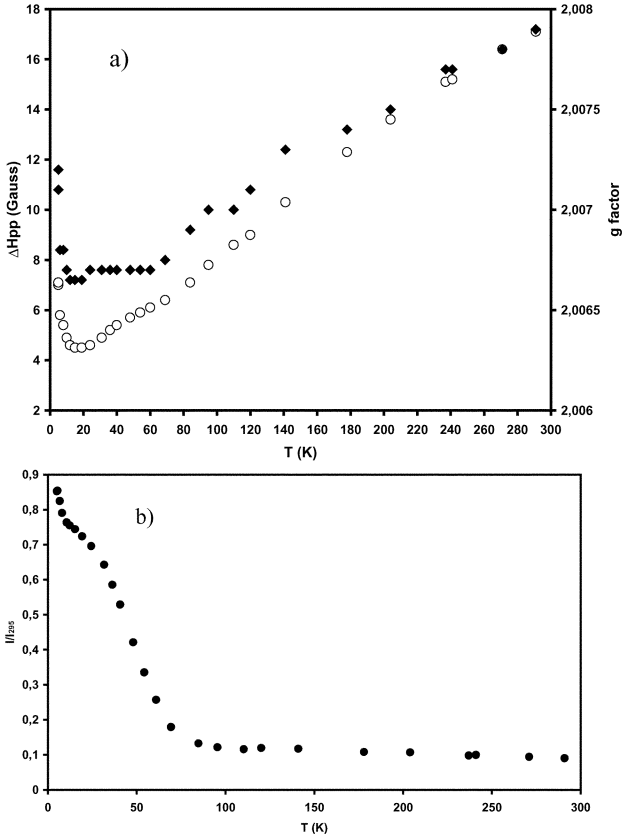

Fig. 15 (a) Temperature dependence of the EPR line width (ΔH_{pp}) (circles) and g factor (black diamonds); (b) normalised spin susceptibility of a single crystal of $(BET\text{-}TTF)_3(ReO_4)_2$ with the magnetic field perpendicular to the conducting *ab* plane.

could also explain the negative or field-independent MR in the low field region ($0 < B < 2$ T) (see Fig. 13).

EPR Measurements

The magnetic properties of the three salts have been studied by electron paramagnetic resonance (EPR) spectroscopy in appropriate single crystals. The values found for the line width (ΔH_{pp}) and the g factor along the three rotation axes are listed in Table 3.

In accordance with the one dimensional character of the $(BET\text{-}TTF)ReO_4$ salt (**1**), the EPR line width is very narrow, in the range 2.5–3.5 Gauss, and the g value variation with the angle gives an average g factor value that is almost the same as those observed for free BET-TTF radical ions in solution.[15] As in other TTF salts, the minimum g value occurs when the magnetic field is along the direction perpendicular to the molecular plane of the BET-TTF (crystallographic *a* axis) and the maximum g value occurs when the magnetic field is parallel to the central C=C bond of BET-TTF.

The variation in the EPR signal intensity with the temperature follows a Curie-like behaviour, in agreement with the electron localisation observed in the transport properties.

In the $(BET\text{-}TTF)_3(ReO_4)_2$ salt (**2**), according to the X-ray and electronic band structures, we should consider two different magnetic subsystems associated with layers 1 and 2 defined in the structural study (see Fig. 2). In layer 1, electrons are moving at a high temperature since the conductivity measurements reveal metallic properties down to $\approx$125 K which are associated with this layer; in contrast, layer 2 consists of localized magnetic moments located in the completely ionized BET-TTF radical ions. Therefore, this salt belongs to a family of metallic radical cation salts with paramagnetic anions that are particularly interesting, since delocalised conduction electrons and localised magnetic moments coexist and offer the possibility of observing new physical phenomena arising from their mutual interaction. In contrast to almost all known systems,[25] which have localised magnetic moments in the inorganic counterion of the salts, compound **2** has a localised magnetic moment in an organic molecule. The only other case of which we are aware is the recently reported salt $(EDT\text{-}TTF\text{-}CONH_2)_2ReO_4$.[26]

The EPR signal of a single crystal of **2** consists of a single line for all orientations of the crystal with respect to the static magnetic field. This fact seems to be indicative of the existence of an interaction between the two magnetic subsystems present in this salt. Such an interaction can be due to a super-exchange mechanism promoted by the short S···O contacts present in the structure of salt **2** between the S atoms of the BET-TTF molecules and the ReO_4^- anions. The variable-temperature EPR studies that were carried out in the temperature range 4–300 K, with the magnetic field perpendicular to the conducting *ab* plane, confirm the above mentioned interaction. Indeed, as the temperature is lowered, the g value does not remain constant but decreases until $\approx$70 K and then remains constant until $\approx$15 K, when a drastic increase in the g value is observed (Fig. 15a). The variation in the g value in the temperature range where the compound is in the metallic regime is a clear indication of the interaction between both magnetic subsystems.[25f]

Upon cooling down, the line width of the EPR signal decreases from 18 Gauss at 295 K to a minimum value of 4.5 Gauss at $\approx$15 K and then it broadens to reach a line width of 7.5 Gauss at 4 K. The decrease is not monotonous since a small change in the slope is observed at around 70 K (Fig. 15a). Within experimental error, the susceptibility is almost temperature independent down to 80 K and then increases showing a variation of the slope at around 15 K (Fig. 15b).

Taking into account all the characteristics of the temperature dependence of the EPR parameters and the conductivity, we can ascribe the first change observed in the EPR parameters to a metal–metal transition produced in the conducting layer 1. The second upturn in the temperature dependence of the EPR parameters at around 15 K is found just below the temperature region where a change in the slope is observed in the conductivity measurements (Fig. 10) and can be attributed to the non-conducting layer 2.

The magnetic properties of salt **3** as studied by EPR spectroscopy are very similar to those of β-like $(BET\text{-}TTF)_2X$ salts with octahedral and linear anions.[7,27] Thus, the line width range is 7.5–12 Gauss and the orientation dependence of the line width is in phase with that of the g value for the three axes of the crystal, as shown in Fig. 16. The values found for ΔH_{pp} when H_o is in the *ab* conducting plane are very similar, in agreement with the electronic structure analysis which indicates

Table 3 EPR-parameters of $(BET\text{-}TTF)_m(ReO_4)_n$ salts at room temperature

	Maximum		Intermediate		Minimum	
Salt	g	ΔH_{pp}/G	g	ΔH_{pp}/G	g	ΔH_{pp}/G
$(BET\text{-}TTF)ReO_4$ (**1**)	2.0108	3.5	2.0065	2.5	2.0021	2.5
$(BET\text{-}TTF)_3(ReO_4)_2$ (**2**)	2.0101	20	2.0070	14	2.0019	12.5
$(BET\text{-}TTF)_9(ReO_4)_4{\cdot}2THF$ (**3**)	2.0098	12	2.0073	8.8	2.0015	7.4

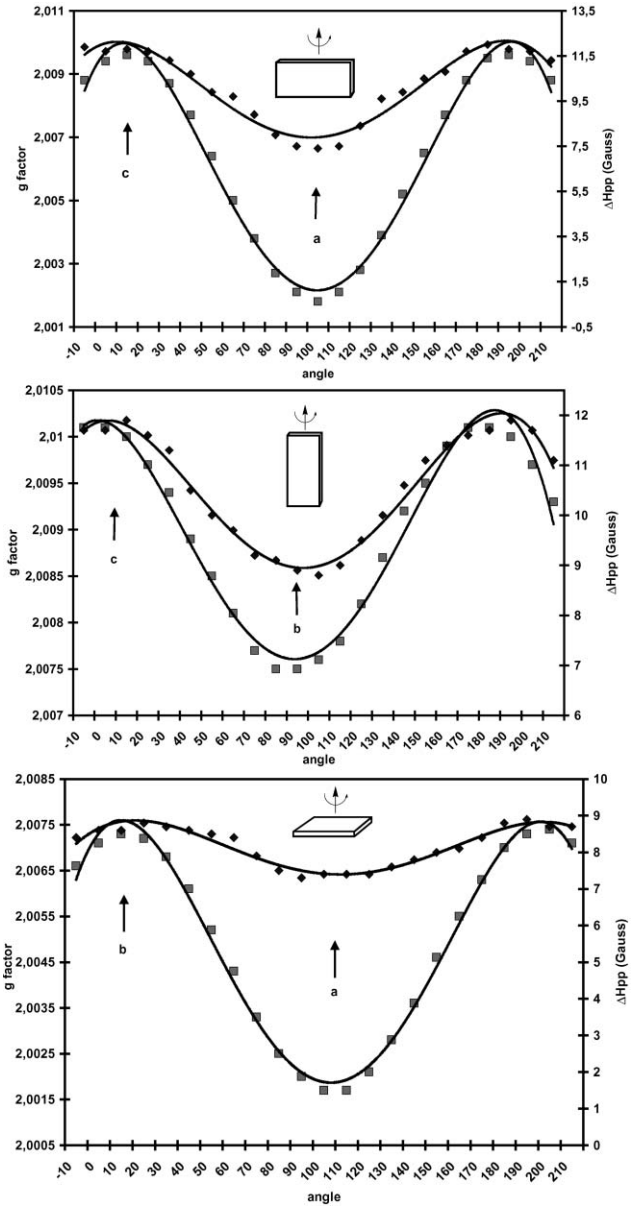

Fig. 16 Angular dependence of EPR line width (ΔH_{pp}) (black diamonds), and *g* factor (black squares) for three different orthogonal rotation planes of $(BET\text{-}TTF)_9(ReO_4)_4{\cdot}2THF$ at room temperature.

that in this 2D structure the $(BET\text{-}TTF)^{1+}$ radicals are strongly interacting. On the other hand, the temperature dependence of the EPR parameters is in accordance with the metallic character of this salt. Thus, the line width decreases smoothly with decreasing temperature and reaches 5 Gauss at 4 K. The *g* value remains constant, and the susceptibility decreases smoothly and gradually without showing any abrupt changes. This behaviour is consistent with a transition to a non-metallic state driven by the localisation of electrons, as it happens in the β phases of $(BET\text{-}TTF)_2XF_6$ (X = P, As, Sb) salts.[7]

Conclusions

Small variation in solvent polarity in the electrocrystallisation of the BET-TTF donor with $n Bu_4NReO_4$ as supporting electrolyte allows the formation of three different salts, $(BET\text{-}TTF)ReO_4$ (**1**), $(BET\text{-}TTF)_3(ReO_4)_2$ (**2**), and $(BET\text{-}TTF)_9(ReO_4)_4{\cdot}2THF$ (**3**). In agreement with the results from X-ray structure determination and electronic structure calculations, the mixed valence salts **2** and **3** exhibit metallic character down to 125 K and 75 K, respectively. A first order phase transition at high pressure (P = 4–5 kbar) has been observed for salt **3**. In order to understand the nature of this phase transition crystal structure analysis under pressure is required. Regarding its magnetic properties, salt **2** is the most interesting candidate. This salt contains delocalised conducting electrons as well as localised magnetic moments located in the two different layers of donors that constitute the salt. The EPR study of this salt indicates that both kinds of electrons are interacting.

The obtained results are also encouraging for the use of other tetrahedral anions in the synthesis of radical cation salts derived from the BET-TTF donor.

Experimental

Synthesis of the radical salts

Crystals of three different radical salts, $(BET\text{-}TTF)ReO_4$ (**1**), $(BET\text{-}TTF)_3(ReO_4)_2$ (**2**) and $(BET\text{-}TTF)_9(ReO_4)_4{\cdot}2THF$ (**3**), were synthesized on a platinum wire electrode by the standard electrochemical oxidation of the BET-TTF donor in a H-shaped cell under low constant current (I = 0.5–1.2 μA) using $n\text{-}Bu_4NReO_4$ as supporting electrolyte. The solvent used and the electrocrystallization times vary depending on the salt. The exact conditions for the synthesis of the radical salts are summarized in Table 1.

X-Ray structure determination (Table 2)‡

Reflections were measured at room temperature with an Enraf-Nonius CAD-4F diffractometer [λ(Mo-K_α) = 0.71073 Å, graphite monochromator, ω-scan]. The structures were solved by a direct method, completed by the Fourier method, using the AREN programs[28] and refined by a least squares technique in the full-matrix anisotropic approximation [$BET{\cdot}ReO_4$ and $(BET)_3(ReO_4)_2$] and anisotropic (Re, S, O atoms)–isotropic approximation [$(BET)_9(ReO_4)_4{\cdot}2(THF)$] for all non-hydrogen atoms by using the SHELXL-93 program.[29] The positions of the hydrogen atoms were introduced geometrically and accounted for in the calculation.

Transport measurements

The in-plane resistance of crystals at ambient pressure was measured by a standard four-probe d.c. method with a constant current of 10 or 100 μA. Resistance and magnetoresistance of samples under quasi-hydrostatic pressure were measured by a four-probe method with an in-plane alternating current of 100 μA at a frequency of v = 137 Hz. A superconducting magnet and a clamp-type piston-cylinder pressure cell filled with Fluorinert FC75 as a pressure medium were used to produce the magnetic field of up to 16 T and pressure of up to 22 kbar, respectively. Pressure inside the cell was measured by the manganin wire gauge. In each experiment two single crystals were measured simultaneously. They were contacted with graphite paste to platinum wires of 20 μ diameter. The pressure in the cell was changed and fixed at room temperature; during cool down to 4.2 K the average pressure drop was of the order of 3 kbar.

Electron paramagnetic resonance

EPR spectra in the range 4–300 K were obtained with an X-Band Bruker ESP 300E spectrometer equipped with a microwave bridge ER041XK, a rectangular cavity operating in T102 mode, a Bruker variable temperature unit and an Oxford ESR-900 cryostat, and a field controller ER 032M system. An

‡CCDC reference numbers 164145, 174645 and 174646. See http://www.rsc.org/suppdata/jm/b1/b106070h/ for crystallographic files in .cif or other electronic format.

automatic goniometer was used to measure the EPR parameters angle dependence.

Band structure calculations

The tight-binding band structure calculations were based upon the effective one-electron Hamiltonian of the extended Hückel method.[30] The off-diagonal matrix elements of the Hamiltonian were calculated according to the modified Wolfsberg–Helmholz formula.[31] All valence electrons were explicitly taken into account in the calculations and the basis set consisted of double-ζ Slater-type orbitals for C and S, and single-ζ Slater-type orbitals for H. The exponents, contraction coefficients and atomic parameters for C, S and H were taken from previous work.[32]

Acknowledgement

This work was supported by DGI-Spain (Projects BQU2000-1157 and BFM2000-1312-C02-01), Generalitat de Catalunya (Projects 2000 SRG 00114 and 1999 SGR 207), CSIC/CONACYT (2001MX0008), NATO (Project GRG.LG. 9743316) and the Russian National Program ''Physics of quantum and wave processes'.

References

1 (*a*) D. Jerome, A. Mazaud, M. Ribault and K. Bechgaard, *J. Phys. Lett.*, 1980, **41**, L95–98; (*b*) K. Bechgaard, K. Carneiro, F. B. Rasmunssen, M. Olsen, G. Rindorf, C. S. Jacobsen, H. J. Pedersen and J. C. Scott, *J. Am Chem Soc.*, 1981, **103**, 2440.

2 (*a*) *The Physics and Chemistry of Organic Superconductors*, ed G. Saito and S. Kagoshima, Springer, Berlin, 1990; (*b*) *Organic Superconductors (Including Fullerenes) Synthesis, Structure, Properties, and Theory*, ed. J. M. Williams, J. R. Ferraro, R. J. Thorn, K. D. Carlson, U. Geiser, H. H. Wang, A. M. Kini and M.-H. Whangbo, Prentice Hall, Englewood Cliffs, New Jersey, 1992; (*c*) R. M. Metzger, in *Advances in Synthetic Metals, Twenty Years of Progress in Science and Technology*, ed P. Bernier, S. Lefrant and G. Bidan, Elsevier, Lausanne, 1999, p. 317.

3 S. S. P. Parkin, E. M. Engler, R. R. Schumaker, R. Lagier, V. Y. Lee, J. C. Scott and R. L. Green, *Phys. Rev. Lett.*, 1983, **50**, 270.

4 J. M. Williams, A. M. Kini, H. H. Wang, K. D. Carlson, U. Geiser, L. K. Montgomery, G. J. Pyrka, D. M. Watkins, J. M. Kommers, S. J. Boryschuk, A. V. Strieby Crouch, W. K. Kwok, J. E. Schirber, D. L. Overmeyer, D. Jung and M.-H. Whangbo, *Inorg. Chem.*, 1990, **29**, 3262.

5 J. J. Novoa, M. C. Rovira, C. Rovira, J. Veciana and J. Tarrés, *Adv. Mater.*, 1995, **7**, 233.

6 (*a*) J. Tarres, J. Veciana and C. Rovira, *Synth. Met.*, 1995, **70**, 1167; (*b*) E. Coronado, L. R. Falvello, J. R. Galán-Mascarós, C. Giménez-Saiz, C. J. Gómez-García, V. N. Laukhin, A. Pérez-Benítez, C. Rovira and J. Veciana, *Adv. Mater.*, 1997, **9**, 984; (*c*) M. Clemente-León, E. Coronado, J. R. Galán-Mascarós, C. Giménez-Saiz, C. J. Gómez-García, J. Vidal-Gancedo, C. Rovira, E. Canadell and V. Laukhin, *Inorg. Chem.*, 2001, **40**, 3526.

7 J. Tarrés, N. Santaló, M. Mas, E. Molins, J. Veciana, C. Rovira, S. Yang, H. Lee, D. O. Cowan, M. L. Doublet and E. Canadell, *Chem. Mater.*, 1995, **7**, 1558.

8 C. Rovira, J. Tarrés, E. Ribera, J. Veciana, E. Canadell, E. Molins, M. Mas, V. Laukhin, M-L. Doublet, D. O. Cowan and S. Yang, *Synth. Met.*, 1997, **86**, 2145.

9 E. Laukhina, E. Ribera, J. Vidal-Gancedo, S. Khasanov, L. Zorina, R. Shibaeva, E. Canadell, V. Laukhin, M. Honold, M. S. Nam, J. Singleton, J. Veciana and C. Rovira, *Adv. Mater.*, 2000, **12**, 54.

10 (*a*) S. S. P. Parkin, E. M. Engler, R. R. Schumaker, R. Lagier, V. Y. Lee, J. Voiron, K. Carneiro, J. C. Scott and R. L. Green, *J. Phys. (Paris)*, 1983, **44**, 791; (*b*) K. Carneiro, J. C. Scott and E. M. Engler, *Solid State Commun.*, 1984, **50**, 477.

11 (*a*) S. S. P. Parkin, E. M. Engler, V. Y. Lee and R. R. Schumaker, *Mol. Cryst. Liq. Cryst.*, 1985, **119**, 375; (*b*) H. Kobayashi, A. Kobayashi, Y. Sasaki, G. Saito and H. Inokuchi, *Chem. Lett.*, 1984, 183.

12 R. R. Schumaker, V. Y. Lee and E. M. Engler, *J. Phys. (Paris)*, 1983, **44**, 1139.

13 (*a*) S. Kahlich, D. Schweitzer, I. Heinen, S. E. Lan, B. Nuber, H. J. Keller, K. Winzer and H. W. Helberg, *Solid State Commun.*, 1991, **8**, 191; (*b*) L. I. Buravov, A. G. Khomenko, N. D. Kush, V. N. Laukhin, A. I. Schegolev, E. B. Yagubskii, L. P. Rozemberg and R. P. Shibaeva, *J. Phys. I*, 1992, **2**, 529.

14 In a previous communication [*Synth. Met.*, 1999, **102**, 1707] the formula (BET-TTF)$_9$(ReO$_4$)$_4$·2H$_2$O was ascribed to this salt, but a more accurate X-ray structural determination showed that this formula was not correct.

15 C. Rovira, J. Veciana, N. Santaló, J. Tarrés, J. Cirujeda, E. Molins, J. Llorca and E. Espinosa, *J. Org. Chem.*, 1994, **59**, 3307.

16 C. Rovira, J. Veciana, J. Tarrés, E. Molins, M. Mas, D. O. Cowan and S. Yang, *Synth. Met.*, 1995, **70**, 883.

17 E. Ribera, C. Rovira, J. Veciana, V. N. Laukhin and E. Canadell, *Synth. Met.*, 1997, **86**, 1993.

18 (*a*) V. E. Korotkov and R. P. Shibaeva, *Kristallografiya*, 1989, **34**, 1442; (*b*) V. E. Korotkov and R. P. Shibaeva, *Sov. Phys. Crystallogr. (Engl. Transl.)*, 1989, **34**, 865.

19 J. Tarrés, M. Mas, E. Molins, J. Veciana, C. Rovira, J. Morgado, R. T. Henriques and M. Almeida, *J. Mater. Chem.*, 1995, **5**, 1653.

20 (*a*) M.-H. Whangbo, J. M. Williams, P. C. W. Leung, M. A. Beno, T. J. Emge and H. H. Wang, *Inorg. Chem.*, 1985, **24**, 3500; (*b*) since overlap is explicitly included in extended Hückel calculations, these interaction energies (β) should not be confused with the conventional transfer integrals (t). The two quantities are obviously related and have the same physical meaning but the absolute values of the β's are somewhat larger than those of the t's.

21 M. V. Kartsovnik, P. A. Kononovich, V. N. Laukhin, A. G. Khomenko and I. F. Schegolev, *Sov. Phys. JETP (Engl. Transl.)*, 1985, **61**, 866.

22 V. Laukhin, A. Pérez-Benítez, C. Rovira, J. Veciana, E. Canadell, A.-K. Klehe and J. Singleton, *Synth. Met.*, 2001, **120**, 1027.

23 A. Audouard, P. Auban-Senzier, V. N. Laukhin, L. Brossard, D. Jerome and N. D. Kushch, *Europhys. Lett.*, 1996, **34**, 599.

24 *Magnetoresistance in Metals*, ed A. B. Pippard, Cambridge University Press, Cambridge, 1989.

25 (*a*) M. Kurmoo, A. W. Graham, P. Day, S. J. Coles, M. B. Hursthouse, J. L. Caulfield, J. Singleton, F. L. Pratt, W. Hayes, L. Ducasse and P. Guionneau, *J. Am. Chem. Soc.*, 1995, **117**, 12209; (*b*) P. Cassoux, *Science*, 1996, **272**, 1277; (*c*) M. Matos, G. Bonfait, R. T. Henriques and M. Almeida, *Phys. Rev. B*, 1996, **54**, 15307; (*d*) H. Kobayashi, H. Tomita, T. Naito, A. Kobayashi, F. Sakai, T. Watanabe and P. Cassoux, *J. Am. Chem. Soc.*, 1996, **118**, 368; (*e*) E. Coronado and J. Gómez-García Carlos, *Chem. Rev.*, 1998, **98**, 273; (*f*) E. Ribera, C. Rovira, J. Veciana, J. Tarrés, E. Canadell, R. Rousseau, E. Molins, M. Mas, J.-P. Schoeffel, J.-P. Pouget, J. Morgado, R. T. Henriques and M. Almeida, *Chem. Eur. J.*, 1999, **5**, 2025; (*g*) E. Coronado, J. R. Galán-Mascarós, J. Gómez-García Carlos and V. Laukhin, *Nature*, 2000, **408**, 447; (*h*) H. Fujiwara, E. Fujiwara, Y. Nakazawa, B.-Zh. Narymbetov, K. Kato, H. Kobayshi, A. Kobayashi, M. Tokumoto and P. Cassoux, *J. Am. Chem. Soc.*, 2001, **123**, 306.

26 K. Heuzé, M. Fourmigué, P. Batail, E. Canadell and P. Auban-Senzier, *Chem. Eur. J.*, 1999, **5**, 2971.

27 C. Rovira, J. Tarrés, E. Ribera, J. Veciana, E. Canadell, E. Molins, M. Mas, V. Laukhin, M.-L. Doublet, D. O. Cowan and S. Yang, *Synth. Met.*, 1997, **86**, 2145.

28 V. I. Andrianov, *AREN-88. The system of Programs for Solving and Refinement of Crystal Structures*, Institute of Crystallography AN SSSR, Moscow, 1988.

29 G. M. Sheldrick, *SHELXL-93, Program for the Refinement of Crystal Structure*, Göttingen University, Germany, 1993.

30 M.-H. Whangbo and R. Hoffmann, *J. Am. Chem. Soc.*, 1978, **100**, 6093.

31 J. Ammeter, H.-B. Bürgi, J. Thibeault and R. Hoffmann, *J. Am. Chem. Soc.*, 1978, **100**, 3686.

32 A. Pénicaud, K. Boubekeur, P. Batail, E. Canadell, P. Auban-Senzier and D. Jérome, *J. Am. Chem. Soc.*, 1993, **115**, 4101.